Terahertz sources based on intracavity frequency mixing in mid-infrared quantum cascade lasers with passive nonlinear sections

Robert W. Adams, Augustinas Vizbaras, Min Jang, Christian Grasse, Simeon Katz et al.

Citation: Appl. Phys. Lett. **98**, 151114 (2011); doi: 10.1063/1.3579260
View online: http://dx.doi.org/10.1063/1.3579260
View Table of Contents: http://apl.aip.org/resource/1/APPLAB/v98/i15
Published by the American Institute of Physics.

Terahertz sources based on intracavity frequency mixing in mid-infrared quantum cascade lasers with passive nonlinear sections

Robert W. Adams,[1] Augustinas Vizbaras,[2] Min Jang,[1] Christian Grasse,[2] Simeon Katz,[2] Gerhard Boehm,[2] Markus C. Amann,[2] and Mikhail A. Belkin[1,a)]
[1]*Department of Electrical and Computer Engineering, The University of Texas at Austin, Austin, Texas 78758, USA*
[2]*Walter Schottky Institut, Technische Universität München, Am Coulombwal 3, 85748 Garching, Germany*

(Received 6 December 2010; accepted 19 March 2011; published online 15 April 2011)

We report the design and performance of terahertz quantum cascade laser sources based on intracavity difference frequency generation in dual-wavelength mid-infrared quantum cascade lasers with a passive nonlinear section at the exit facet, designed for giant second-order nonlinear susceptibility. These devices operate in the mid-infrared at $\lambda_1=8.4$ μm and $\lambda_2=9.5$ μm, with terahertz output at the difference frequency, $\lambda_3\approx 73$ μm. Terahertz output of approximately 100 nW was observed up to a heat sink temperature of 210 K. © *2011 American Institute of Physics*. [doi:10.1063/1.3579260]

The terahertz (THz) spectral range ($\lambda=30-300$ μm) still lacks a compact electrically pumped room temperature semiconductor source. Cryogenic cooling is still necessary for operation of THz quantum cascade lasers (QCLs) (Refs. 1 and 2). We have recently demonstrated that THz QCL sources based on intracavity difference-frequency generation (DFG) in dual-wavelength mid-infrared (mid-IR) QCLs may present a viable alternative to THz QCLs for generating THz radiation at room temperature.[3,4]

Devices in Refs. 3 and 4 utilized active regions with optical nonlinearity integrated with laser transitions. The benefits of this approach are that laser modes have good spatial overlap with the nonlinear section and that no optical loss is introduced in the laser cavity by the resonant optical nonlinearity.[3,4] However, the value of the nonlinear susceptibility ($\chi^{(2)}$) in this approach is determined by the population inversion across the laser transition, which is clamped to values $\Delta N\approx 2\times 10^{15}$ cm^{-3} at the laser threshold.[4] Additionally, resonant optical nonlinearity with population inversion will intrinsically have transitions at two laser frequencies, which leads to gain competition between mid-IR pump modes.[5]

Here we present an alternative design of THz QCL sources based on DFG. Devices use a passive nonlinear section at the exit facet, designed to have resonant $\chi^{(2)}$. Theoretical analysis shows that this design of THz DFG QCL sources may lead to higher THz conversion efficiencies compared to that in devices based on optical nonlinearity with population inversion, while producing only minor additional losses to the pump lasers. Experimentally, our proof-of-principle devices produced approximately 100 nW of output power at a frequency of 4.1 THz up to 210 K with a conversion efficiency of 0.5 μW/W^2. As discussed below, the power conversion efficiency of these lasers is expected to improve by over two orders of magnitude in fully-optimized structures.

The details of our device design are shown in Fig. 1(a). A nonlinear layer (NL) tailored to have resonant $\chi^{(2)}$ for DFG, is grown on top of a QCL active region. The NL is 500 nm thick and is comprised of 16 repetitions of the structure shown in Fig. 1(b). The active region consists of 3.1 μm of double-phonon resonance[6] QCL structures designed to emit at $\lambda_1=8.4$ μm and $\lambda_2=9.5$ μm, with 25 and 23 repetitions each, respectively. Devices were grown by molecular beam epitaxy on an InP substrate, n-doped to 6×10^{16} cm^{-3}. The growth initially ended at the NL. The NL was then selectively removed to leave 50–200 μm long sections near the exit facet to reduce optical losses for the pumps. THz radiation generated more than 200 μm away from the exit facet is completely absorbed by free-carriers in mid-IR QCLs. The NL sections were further patterned with 10 μm-wide trenches every 50 μm, see Fig. 1(a), to facilitate current transport to the active region below. An InP upper waveguide cladding (4-μm-thick and 200-nm-thick layers of InP, n-doped to 4×10^{16} cm^{-3} and 5×10^{18} cm^{-3}, respectively, followed by a 50-nm-thick layer of GaInAs n-doped 2×10^{19} cm^{-3}) is then overgrown. The devices are processed into 25 μm wide ridges with tapered sections 60 μm wide, similarly to that in Ref. 4.

To demonstrate the advantages of a "passive nonlinear scheme" for edge-emitting devices we compare the expected THz DFG conversion efficiency of a device outlined above with that of THz DFG QCL source in Ref. 4. The power of the THz DFG output at frequency ω_3 in QCL waveguides is given by the expression:[3,4,8,9]

$$W(\omega_3=\omega_1-\omega_2)=\frac{\omega_3^2}{8\varepsilon_0 c^3 n(\omega_1)n(\omega_2)n(\omega_3)}|\chi^{(2)}|^2\frac{W(\omega_1)W(\omega_2)}{S_{eff}}l_{eff}^2, \quad (1)$$

where $W(\omega_i)$ and $n(\omega_i)$ are the power and refractive index of the beam at frequency ω_i. The term l_{eff} is the effective length of the nonlinear interaction and is given as:

$$l_{eff}^2=\left|\int_0^L \exp\{i[\tilde{k}_{\omega 3}-(\tilde{k}_{\omega 1}-\tilde{k}_{\omega 2})]z\}dz\,\exp[-\tilde{k}_{\omega 3}L]\right|^2=\frac{e^{-\alpha_{\omega 3}L}(e^{-\Delta\tilde{k}L}-1)^2}{(\Delta\tilde{k})^2}, \quad (2)$$

where L is the length of the nonlinear section, $\Delta\tilde{k}=\tilde{k}_{\omega 3}$

a)Electronic mail: mbelkin@ece.utexas.edu.

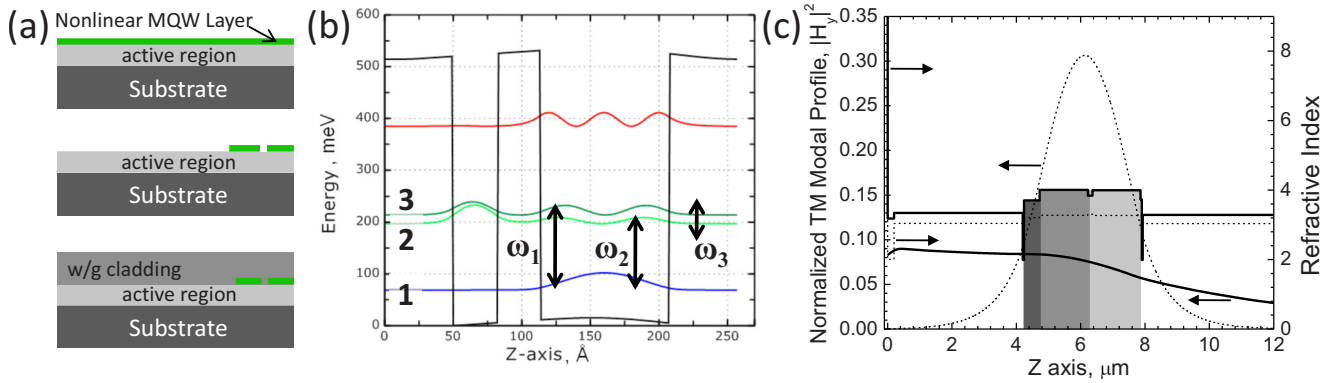

FIG. 1. (Color online) (a) Schematic of device design and processing. The top panel shows a longitudinal cross sectional view of the QCL structure with NL grown above the active region. The subsequent panels (top to bottom) show the selective removal of the NL, and regrowth of the upper waveguide cladding. (b) Conduction band diagram of one period of the passive NL. The layer sequence (in nanometers) is **10**/3.3/**3.1**/9.4, with AlInAs barriers shown in bold. The center 6 nm of the 10 nm barrier is doped n-type to 3×10^{17} cm^{-3}. The energy separation between levels and transition dipole matrix elements for the structure are: E_{12}=128 meV, E_{13}=145 meV, E_{23}=17 meV, z_{12}=1.63 nm, z_{13}=1.49 nm, z_{23}=4.59 nm. (c) The magnetic field intensity of the TM_{00} mode (left axis) and refractive index profile (right axis) for the λ_1=9.5 um (thin dashed line) and λ_3=73 um (thick solid line) propagating modes in the waveguide. The active regions for each pump are shown in light gray (λ_1=8.4 μm) and gray (λ_2=9.5 μm), and the nonlinear region is shown in dark gray.

$-(\tilde{k}_{\omega1}-\tilde{k}_{\omega2})$, $\tilde{k}_{\omega i}=k_{\omega i}+i\alpha_{\omega i}/2$ are complex propagation constants of the beams at ω_i with $k_{\omega i}$ being the real part of $\tilde{k}_{\omega i}$ and $\alpha_{\omega i}$ being the power loss (or gain, if negative) of the beams at ω_i. The S_{eff} term is the effective area of interaction of the beams.[3,8] The refractive index and calculated profiles for mid-IR and THz modes in our devices are shown in Fig. 1(c). This data is used to calculate $S_{eff}\approx1.92\times10^5$ μm^2 for a 60-μm-wide waveguide. In comparison, the value of S_{eff} for devices in Ref. 4 is only 4×10^3 μm^2, owing to good modal overlap with the nonlinear section. Assuming perfect phase-matching $\Delta k=0$, the value of l_{eff} for devices in Ref. 4 is then determined only by the THz losses, $l_{eff}=1/\alpha_{\omega3}$ =80 μm. Assuming the same THz losses $\alpha_{\omega3}\approx250$ cm^{-1} in our current device and the optical losses due to resonant absorption in the nonlinear section for the TM_{00} mid-IR pump modes of $\alpha_{\omega1}\approx102$ cm^{-1} and $\alpha_{\omega2}\approx95$ cm^{-1}, Eq. (2) is maximized for $L\approx85$ μm to produce $l_{eff}\approx31$ μm. We note that an 85-μm-long nonlinear section will increase the total loss for the pumps in our devices by 2.3 cm^{-1}, cf., Eq. (5). The waveguide loss for mid-IR pumps in a laser without optical nonlinearity is estimated to be $\alpha_{LAS}\approx9$ cm^{-1}. Thus, the presence of an 85-μm-long nonlinear section in a 3-mm-long laser is only expected to increase the total loss (including mirror loss estimated to be 2.1 cm^{-1}) for mid-IR pumps by less than 25%.

For resonant DFG based on intersubband transitions, the expression for $\chi^{(2)}$ simplifies to[3,4,8,9]

$$\chi^{(2)}(\omega_3=\omega_1-\omega_2)=\frac{e^3}{\hbar^2\varepsilon_o}\frac{z_{12}z_{23}z_{31}}{(\omega-\omega_{32}+i\Gamma_{32})}\times\left[\frac{N_1-N_3}{(\omega_1-\omega_{13}+i\Gamma_{31})}+\frac{N_1-N_2}{(-\omega_2+\omega_{12}+i\Gamma_{21})}\right] \quad (3)$$

where N_i is the electron population density in state i, and ez_{ij}, ω_{ij}, and Γ_{ij} are the dipole matrix element, frequency, and transition linewidth broadening between states i and j. For the passive nonlinear section, we assume that all electron population is in the ground state "1" and $N_1-N_3=N_1-N_2=N\approx7\times10^{16}$ cm^{-3}. We assume a transition linewidth of 7.5 meV for the active design, and 5 meV for the passive design. The dedicated nonlinear section of the passive design should have a narrower linewidth due to the decreased number of interacting states, cf. Refs. 10 and 11. We obtain $|\chi^{(2)}|=1.08\times10^6$ pm/V for the passive design. This needs to be compared with $|\chi^{(2)}|=4\times10^4$ pm/V for the active design.[4]

Solving Eq. (1) using the calculated values of l_{eff}, S_{eff}, and $|\chi^{(2)}|$ for the passive and active designs, and using the effective refractive indices $n(\omega_1)\approx n(\omega_2)\approx n(\omega_3)\approx3.2$ we obtain the conversion efficiency $\eta=W_3/W_1W_2\approx63$ μW/W^2 for the passive design and ≈40 μW/W^2 for the active design in Ref. 4. Thus, passive devices have the potential to produce stronger THz output.

Measurements of the proof-of-principle devices were taken using 100 ns current pulses at 100 kHz repetition rate for gathering mid-IR data, and 400 ns pulses at 50 kHz for gathering THz data. Off-axis parabolic mirrors were used to collect and refocus laser output onto a thermopile detector or a calibrated He-cooled Si bolometer for mid-IR and THz measurements, respectively. Optical filters were used to distinguish between the power outputs at different frequencies. Mid-IR and THz power data was corrected for the 32% and ~10% collection efficiency of our setup, respectively. Lasers with 1.8 mm and longer laser cavities provided dual-wavelength mid-IR output up to room temperature.

Experimentally, the best THz performance was achieved with a 1.8-mm-long laser ridge with a nonlinear section length of 175 μm. THz emission was observed from this device up to 210 K, as seen in Fig. 2(a). The spectral position and shape of the THz output was in good agreement with mid-IR pump spectra, see Fig. 2(a). The THz peak power output at 80 K was measured to be approximately 100 nW. THz power measurements at higher temperatures were difficult because of the strong thermal background, cf., Fig. 2(a) for THz emission at 210 K. The light-output versus current density for mid-IR pumps of a device described above and a device with identical dimensions without a nonlinear section are shown in Fig. 2(b) for 80 K operation and Fig. 2(c) for 210 K operation. The threshold current densities for both pumps in the device with 175-μm-long nonlinear section were approximately 25% higher than that in the device without the nonlinear section at 80 K and 210 K, respectively. However, devices with 175-μm-long nonlinear section are expected to have the total loss for ω_1 and ω_2 of 22 cm^{-1} and 21 cm^{-1}, respectively, which are 65%–75% higher than

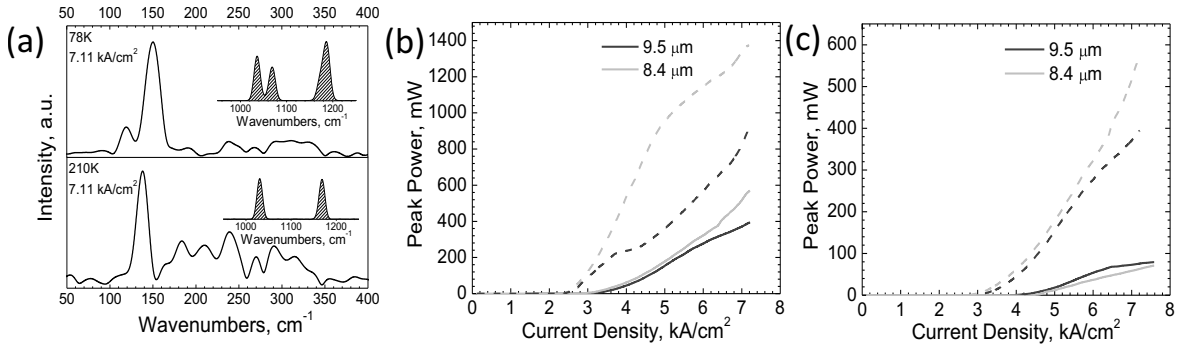

FIG. 2. (a) THz spectra at both 78 and 210 K of a device with high-reflectivity back facet coating and nonlinear section length of 175 μm. Emission centered at $\omega_3 \approx 4.2$ THz. Inset shows the emission spectra for the mid-IR pumps, $\lambda_1 \approx 8.4$ μm and $\lambda_2 \approx 9.5$ μm. (b) Pump intensities vs current density for a section without nonlinear section (dashed lines) and with nonlinear tapered section 175 μm in length (solid lines). Both samples are high reflectivity back facet coated, with ridges 1.8 mm $\times$ 25 μm, tested at a heat sink temperature of 78 K, with 100 kHz 100 ns pulses. (c) Pump intensities vs current density for the same ridge with nonlinear section length 175 um in length, at heat sink temperature of 78 K (dashed line) and 210 K (solid line).

that for a device without nonlinearity. Experimental results indicate that the nonlinear losses are smaller than what was calculated. We believe this may be partly due to smaller-than-expected doping in the nonlinear sections and partly due to transitions in the nonlinear section slightly off-resonance with the mid-IR pump frequencies. Smaller-than-expected electron concentrations in $Ga_{0.47}In_{0.53}As/Al_{0.48}In_{0.52}As/InP$ heterostructures, modulation doped in $Al_{0.48}In_{0.52}As$ barriers, were previously observed and the effect has been attributed to deep electron trapping centers in Si-doped $Al_{0.48}In_{0.52}As$.[12–14] We note that we have recently observed similar smaller-than-expected losses in our nonlinear QCLs designed for second-harmonic generation.[15]

Given the maximum output power of the pumps shown in Fig. 2(b) and 100 nW THz power output at 78 K, we can estimate the *external conversion efficiency* of our device to be $\eta_{ext}=0.5$ $\mu W/W^2$. The value of η_{ext} is related to the DFG conversion efficiency introduced earlier by:

$$\eta_{ext} = \frac{T_3}{T_1 T_2 e^{-L_{NL}(\alpha_{\omega 1}+\alpha_{\omega 2})}}\eta, \tag{4}$$

where T_i is power transmission through the exit facet for the beam at frequency ω_i. Assuming $T_1=T_2\approx 0.7$, and $T_3 \approx 0.15$,[7] this expression leads to a theoretical value of $\eta_{ext}=330$ $\mu W/W^2$ in devices with $L_{NL}=175$ μm.

The discrepancy between our measured external conversion efficiency and calculated external conversion efficiency is likely to be the result of several factors. First, lower than nominal doping level in the nonlinear section leads to lower conversion efficiencies. Assuming three times lower doping level in the nonlinear section, we obtain $|\chi^{(2)}|=3.59\times 10^5$ pm/V, $l_{eff}=44$ μm (limited primarily by THz losses) for the nonlinear section length of 175 μm, and $\eta_{ext}=18.7$ $\mu W/W^2$. Second, our DFG process is likely to be not perfectly phasematched. In particular, increasing the substrate doping concentration by 4×10^{16} cm^{-3} will lead to a change in phase mismatch of $\Delta k=58$ cm^{-1} and an increase in THz losses to $\alpha_{\omega 3}=450$ cm^{-1} which will result in η_{ext} to drop further to 7.23 $\mu W/W^2$. Other factors may reduce the conversion efficiency further, including: the pumps being off-resonance with the transitions in the NL, the transition linewidth being larger than that assumed for the calculations, and mid-IR pumps operating in higher-order lateral modes.

Future work will focus on device optimization to achieve conversion efficiencies close to those predicted theoretically and on improving device design to achieve higher conversion efficiencies. Detailed theoretical simulations that include effects of non-uniform optical pumping and optical transition saturation in the NL predict that devices with fully-resonant passive nonlinear structures and improved THz radiation outcoupling using a microlens[4,16] can provide over 100 μW of THz DFG output at room temperature using mid-IR pumps with $W_1=W_2=2W$.[17]

The University of Texas group acknowledges support from the Texas Higher Education Coordinating Board "Norman Hackerman Advanced Research Program" award and National Science Foundation Grant No. ECCS-0935217. Walter Schottky Institut group acknowledges financial support from the excellence cluster "Nano Initiative Munich (NIM)."

[1]S. Kumar, Q. Hu, and J. L. Reno, Appl. Phys. Lett. **94**, 131105 (2009).
[2]R. W. Adams, K. Vijayraghavan, Q. J. Wang, J. Fan, F. Capasso, S. P. Khanna, A. G. Davies, E. H. Linfield, and M. A. Belkin, Appl. Phys. Lett. **97**, 131111 (2010).
[3]M. A. Belkin, F. Capasso, A. Belyanin, D. L. Sivco, A. Y. Cho, D. C. Oakley, C. J. Vineis, and G. W. Turner, Nat. Photonics **1**, 288 (2007).
[4]M. A. Belkin, F. Capasso, F. Xie, A. Belyanin, M. Fischer, A. Wittmann, and J. Faist, Appl. Phys. Lett. **92**, 201101 (2008).
[5]M. Geiser, C. Pflügl, A. Belyanin, Q. J. Wang, N. Yu, T. Edamura, M. Yamanishi, H. Kan, M. Fischer, A. Wittmann, J. Faist, and F. Capasso, Opt. Express **18**, 9900 (2010).
[6]J. Faist, D. Hofstetter, M. Beck, T. Aellen, M. Rochat, and S. Blaser, IEEE J. Quantum Electron. **38**, 533 (2002).
[7]S. Kohen, B. S. Williams, and Q. Hu, J. Appl. Phys. **97**, 053106 (2005).
[8]C. Gmachl, A. Belyanin, D. L. Sivco, M. L. Peabody, N. Owschimikow, A. M. Sergent, F. Capasso, and A. Y. Cho, IEEE J. Quantum Electron. **39**, 1345 (2003).
[9]R. W. Boyd, *Nonlinear Optics*, 3rd ed. (Academic, Burlington, MA, 2008).
[10]A. Wittmann, Y. Bonetti, J. Faist, E. Gini, and M. Giovannini, Appl. Phys. Lett. **93**, 141103 (2008).
[11]C. Sirtori, F. Capasso, J. Faist, L. N. Pfeiffer, and K. W. West, Appl. Phys. Lett. **65**, 445 (1994).
[12]W.-P. Hong, S. Dhar, P. K. Bhattacharya, and A. Chin, J. Electron. Mater. **16**, 271 (1987).
[13]N. Nakashima, S. Nojima, Y. Kawamura, and H. Asahi, Phys. Status Solidi A **103**, 511 (1987).
[14]J. K. Zahurak, A. A. Iliadis, S. A. Rishton, and W. T. Masselink, J. Appl. Phys. **76**, 7642 (1994).
[15]M. Jang, R. W. Adams, J. X. Chen, W. O. Charles, C. Gmachl, L. W. Cheng, F.-S. Choa, and M. A. Belkin, Appl. Phys. Lett. **97**, 141103 (2010).
[16]A. W. M. Lee, Q. Qin, S. Kumar, B. S. Williams, Q. Hu, and J. L. Reno, Opt. Lett. **32**, 2840 (2007).
[17]Y.-H. Cho, M. A. Belkin, and A. A. Belyanin (unpublished).